The roles of MCDW and deep water iron supply in sustaining a recurrent phytoplankton bloom on central Pennell Bank (Ross Sea)

Citation	Kustka, A. B., Kohut, J. T., White, A. E., Lam, P. J., Milligan, A. J., Dinniman, M. S., ... & Measures, C. I. (2015). The roles of MCDW and deep water iron supply in sustaining a recurrent phytoplankton bloom on central Pennell Bank (Ross Sea). Deep Sea Research Part I: Oceanographic Research Papers, 105, 171-185. doi:10.1016/j.dsr.2015.08.012
DOI	10.1016/j.dsr.2015.08.012
Publisher	Elsevier
Version	Version of Record
Terms of Use	http://cdss.library.oregonstate.edu/sa-termsofuse

Deep-Sea Research I 105 (2015) 171–185

Contents lists available at ScienceDirect

Deep-Sea Research I

journal homepage: www.elsevier.com/locate/dsri

The roles of MCDW and deep water iron supply in sustaining a recurrent phytoplankton bloom on central Pennell Bank (Ross Sea)

Adam B. Kustka [a,*], Josh T. Kohut [b], Angelicque E. White [c], Phoebe J. Lam [d], Allen J. Milligan [e], Michael S. Dinniman [f], Stefanie Mack [f], Elias Hunter [b], Michael R. Hiscock [g], Walker O. Smith Jr. [h], Chris I. Measures [i]

[a] Department of Earth and Environmental Sciences Rutgers University – Newark, 101 Warren Street, Newark, NJ 07102, United States
[b] Department of Marine and Coastal Sciences, Rutgers University – New Brunswick, 71 Dudley Road, New Brunswick, NJ 08901, United States
[c] College of Earth, Ocean & Atmospheric Sciences, Oregon State University, Corvallis, OR 97331, United States
[d] Department of Ocean Sciences, University of California, Santa Cruz, 1156 High Street, Santa Cruz, CA 95064, United States
[e] Department of Botany, Oregon State University, Corvallis, OR 97331, United States
[f] Center for Coastal Physical Oceanography, Old Dominion University, Norfolk, VA 23529, United States
[g] Office of Research and Development, U.S. Environmental Protection Agency, 1200 Pennsylvania Avenue NW, Mail Stop 8726-P, Washington, DC 20460, United States
[h] Virginia Institute of Marine Sciences, College of William & Mary, Gloucester Point, VA 23062, United States
[i] Department of Oceanography, University of Hawaii, 1000 Pope Road, Honolulu, HI 96822, United States

ARTICLE INFO

Article history:
Received 25 January 2015
Received in revised form
24 June 2015
Accepted 27 August 2015
Available online 18 September 2015

Keywords:
Phytoplankton
Ross Sea
Iron demand
Upwelling
Regional ocean modeling system

ABSTRACT

During January–February 2011 standing stocks of phytoplankton (chl *a*) in the Pennell Bank region of the Ross Sea were variable over 10–100 km spatial scales. One area of elevated chl *a* on central Pennell Bank (CPB) appeared to be a recurrent mid-summer feature. The western flank (WF) of Pennell Bank had pronounced signatures of Modified Circumpolar Deep Water (MCDW). We evaluated the spatial extent of Fe limitation and net primary production and tested whether MCDW may provide elevated amounts of Fe to the CPB region, through a combination of in situ measurements, shipboard incubations and a horizontally resolved physical model. Regional fluxes of dissolved Fe from deep to surface waters were compared to calculated Fe demands. Low in situ variable to maximum fluorescence (F_v/F_m; 0.24–0.37) and surface water dissolved Fe concentrations (~0.12–0.21 nM) were suggestive of widespread limitation, corroborated by the consistent responses (F_v/F_m, growth, and nutrient removal ratios) of incubation treatments to Fe addition. MCDW from the WF region had lower dissolved Fe concentrations than that measured in CDW (Circumpolar Deep Water), which suggests on-shelf modification with Fe deplete surface waters and is consistent with the lack of stimulation due to incubation amendments with filtered MCDW. Model results and empirical data suggest MCDW from the WF region is further modified and mixed en route to the CPB region, leading to both the erosion of the canonical MCDW signature and an elevated dissolved Fe inventory of CPB region deep water. This suggests the addition of Fe possibly via diagenesis, as suggested by Marsay et al. (2014). Calculated deep water supply rates to the surface waters of CPB were ~0.18–0.43 m d^{-1}, while calculated rates at the WF or northern Pennell Bank (NPB) regions were negative. The CPB populations exhibited ~4.5-fold higher net production rates compared to those in the WF and NPB regions and required 520–3200 nmol Fe m^{-2} d^{-1}. The modeled vertical supply rates seem to provide ~2–15% of the estimated Fe requirement. Since this flux is based on subsurface dissolved Fe inventories, it does not account for any bioavailable Fe from deep water particulate sources or for Fe recycling in the upper water column. These data suggest the recurrent productivity hotspots at CPB are not fueled by Fe-rich MCDW but are partially supported by the delivery of Fe through vertical exchange processes.

* Corresponding author.
E-mail address: kustka@andromeda.rutgers.edu (A.B. Kustka).

http://dx.doi.org/10.1016/j.dsr.2015.08.012
0967-0637/

1. Introduction

The Ross Sea is one of the most productive regions in the Southern Ocean (Arrigo et al., 1998). A recurring feature of the southern Ross Sea is one of a massive spring bloom that declines in summer well before irradiance or macronutrients become limiting (Smith et al., 2000). Previous studies suggest that the late December decline of biomass (Smith et al., 2000, 2011; Smith and Asper, 2001) is a result of decreased growth due to iron limitation (Olson et al., 2000; Cochlan et al., 2002) coupled with increased rates of loss. As the polynya first opens up in the open Ross Sea, surface water dissolved iron concentrations can be as high as ~4 nM (Sedwick et al., 2000), but these values can be rapidly drawn down early in the season by blooms dominated by *Phaeocystis antarctica* (Sedwick et al., 2011) leading to iron limitation of growth throughout the summer season. Iron-addition experiments have also clearly demonstrated the role of iron in controlling summer growth in the Ross Sea (Sedwick et al., 1997, 2000; Olson et al., 2000). The northern Ross Sea appears to be less productive per annum, as it is ice covered for substantially longer (Arrigo and Van Dijken, 2004), but has not been as extensively studied.

There is substantial spatial and temporal variability in phytoplankton standing stocks in the Ross Sea (Smith et al., 2011). Satellite observations (Arrigo et al., 2008; Smith and Comiso, 2008) and shipboard observations (Smith et al., 2000) demonstrate mid-summer blooms in "open water" regions of the Ross Sea, where Fe is not likely supplied from melting fast ice (Sedwick and DiTullio, 1997) or aeolian input (Winton et al., 2014). Intrusions of relatively Fe rich deep waters may support the heterogeneous distributions of productivity. One source of such deep water in the Southern Ocean, the Upper Circumpolar Deep Water (UCDW), has been shown to enhance biological production near the western Antarctic Peninsula (Prézelin et al., 2000) and within the Antarctic Circumpolar Current (Hiscock et al., 2003). UCDW is relatively old water supplied primarily from the eastern South Pacific Ocean and western Indian Ocean and is characterized by an oxygen minimum

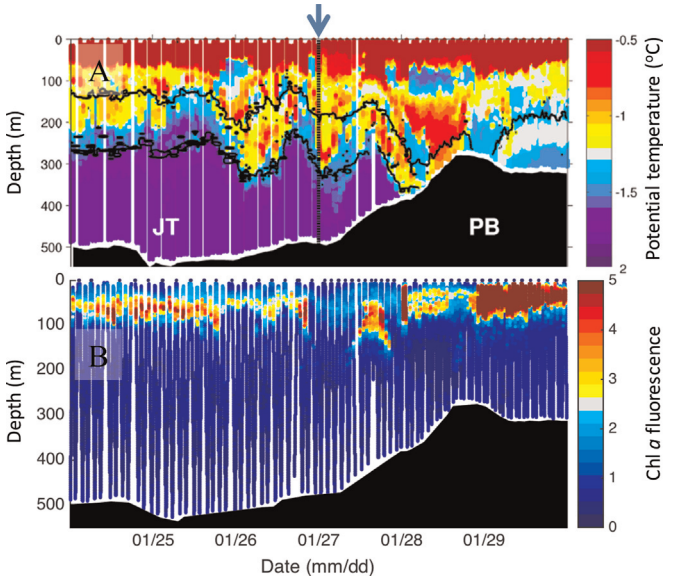

Fig. 2. Glider depth profiles of chl *a* fluorescence and temperature across Pennell Bank and Joides Trough during the cruise. Glider track is shown in red in Fig. 1a. (A) Potential temperature. Black lines indicate neutral density contours at 28 and 28.27, indicative of Modified Circumpolar Deep Water. The arrow shown denotes the point at which the glider changed course from a northeastern heading (along Joides Trough) to a southward trajectory onto Pennell Bank (Fig. 1a). (B) Chl *a* fluorescence. (For interpretation of the references to color in this figure legend, the reader is referred to the web version of this article.)

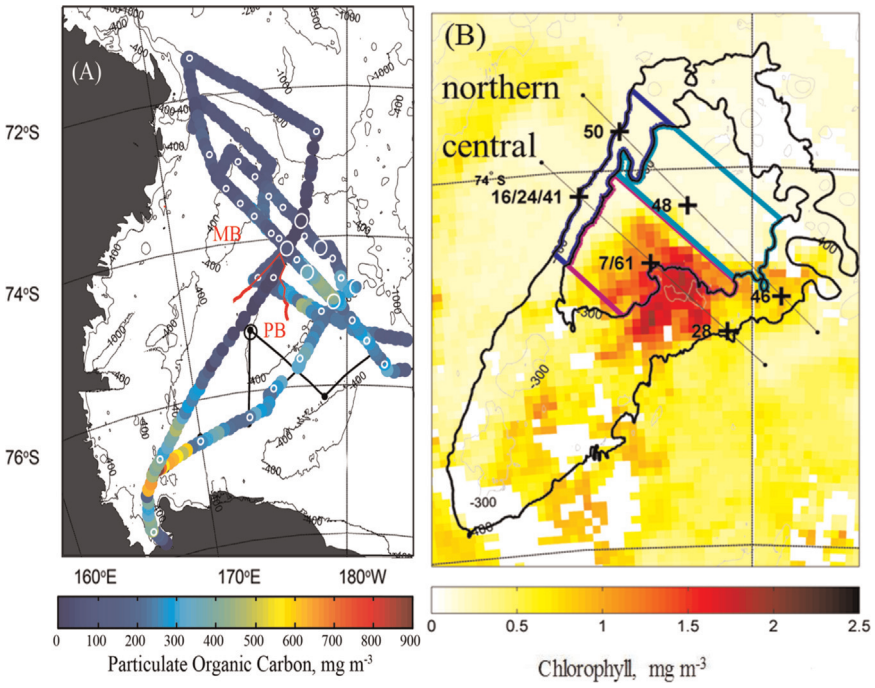

Fig. 1. Particulate organic carbon and satellite-derived chlorophyll *a* along sampling locations during the SEAFARERS expedition. Abbreviations: MB=Mawson Bank, PB=Pennell Bank. (A) Glider track (red lines) and cruise track (highlighted by underway particulate organic carbon measurements via hyperspectral attenuation, except where system was not operational – indicated by the black line). Stations sampled less and more intensively are shown as small and large circles, respectively. (B) MODIS derived chlorophyll *a* concentration relative to Pennell Bank bathymetry and select stations. Composite chlorophyll *a* concentrations from 24 to 27 Jan 2011 are divided into three regions. The western flank (WF, outlined in blue) identifies a region between 300 and 400 m isobath, while central Pennell Bank (CPB; green) and northern Pennell Bank (NPB, purple) indicate waters ≤300 m. In situ variable to maximum chl *a* fluorescence, station Si:N removal ratios, as well as 6 year historical mid-summer chlorophyll levels (2008–2013; MODIS) were sampled across the transects (northern and central) shown here. Incubation stations (7, 16, 24, and 48) and other stations of interest are shown. (For interpretation of the references to color in this figure legend, the reader is referred to the web version of this article.)

and a thermal maximum (Whitworth and Nowlin, 1987; Park et al., 1993). In the Ross Sea, another component of CDW (Lower Circumpolar Deep Water; LCDW) mixes with Antarctic Surface Water to form Modified Circumpolar Deep Water with a range of neutral densities (28–28.27; Jacobs and Giulivi, 1998; Orsi and Wiederwohl, 2009). MCDW flows south onto the shelf along the eastern side of deeper troughs/the western side of banks (Orsi and Wiederwohl, 2009; Dinniman et al., 2003; Kohut et al., 2013) and is further modified along a counter-clockwise pathway around the bank by mixing with surface waters above and denser High Salinity Shelf Water (HSSW) below (Kohut et al., 2013; Dinniman et al., 2003).

We observed a high biomass region over Pennell Bank from Jan–Feb 2011 (Fig. 1) and the concurrent distinct expression of subsurface MCDW along the bank's western boundary (Fig. 2). Given the chronic mid-summer iron limitation, we hypothesized the elevated biomass on Pennell Bank may be explained by iron supplied from MCDW. If so, this should be a recurrent phenomenon because the dynamics of mid and deep water transport to Pennell Bank is driven by topographic steering and geostrophic forces (Kohut et al., 2013). MCDW may provide Fe to Pennell Bank by at least one of two complementary mechanisms. First, the hydrodynamics may support an increased supply of deep waters, including those containing constituents of MCDW, to surface waters on Pennell Bank; with adequate vertical velocity over the shallows of the bank, the dissolved iron inventory of deep water Fe sources need not be elevated. Second, these deep waters may entrain Fe released from sediments around the bank as they are further modified, increasing the Fe concentration. In this scenario, a higher iron flux could be achieved without increasing the vertical velocity. This second possibility includes dissolved Fe sourced from benthic diagenesis as well as resuspension and transport of particulate labile Fe species.

These two mechanisms of iron supply to Pennell Bank were tested during an interdisciplinary sampling campaign dubbed the SEAFAReRS (Slocum Enhanced Adaptive Fe Algal Research in the Ross Sea) cruise. To determine whether this bloom was a persistent or ephemeral feature, we analyzed historical MODIS chl *a* data across the study region. During the cruise, water column physical measurements documented the extent and spatio-temporal dynamics of MCDW (Smith et al., 2014; Kohut et al., 2013), while dissolved Fe profiles characterized the relationship between various water masses and dissolved Fe and were also used to calculate the Fe demand in surface waters at discrete stations. The relative Fe status of phytoplankton populations were determined in ambient waters, as well as during incubation experiments in which populations were amended with iron and with deep waters from various sources. Rates of net primary productivity were measured and the resultant areal productivity was combined with estimated Fe:C ratios to calculate the Fe demands of extant assemblages. In addition, a circulation model was employed to obtain estimates of Fe supply through vertical mixing, as well as estimates of the contribution of CDW to surface waters of Pennell Bank.

2. Materials and methods

2.1. MODIS-Aqua satellite chlorophyll measurements

NASA Moderate Resolution Imagine Spectroradiometer Aqua (MODIS-A) mapped, 8-day, 9 km, standard chl *a* estimates ($\mu g\ L^{-1}$) from the 2013 MODIS-A Reprocessing 2013.1 were downloaded from http://oceandata.sci.gsfc.nasa.gov for 2008–2013. Seven 8-day chlorophyll composites from January 1–February 25 along two 5 pixel wide (~46 km) swaths centered on 54 section-long northern (73° 37.5′ S, 176° 52.5′ E to 74° 52.5′ S, 178° 42.5′ W) and central (73° 57.5′, 175° 57.5′ E to 75° 2.5′ S, 179° 37.5′ W) transects across Pennell Bank were collected (Fig. 1B). There was significant year to year variability in total chlorophyll across the region (Supplemental Fig. 1, Supplemental Table 1), possibly due to differences in physical forcing and timing of ice melt. To account for this, each observation within a season was normalized to the average value from both transects during that season. Then the six year average from each section was calculated. For clarity of presentation, the running average over 5 sections were plotted along each transect.

2.2. Cruise transect and underway measurements

A ship survey was completed from the *RVIB Nathaniel B. Palmer* and sampled the banks and troughs of the outer shelf in the northwestern Ross Sea (Fig. 1), with an emphasis on two transects across Pennell Bank. Measurements of photosynthetically active radiation (PAR) were taken continuously with a BSI QSR-240 sensor positioned on the mast. Underway parameters, including particulate organic carbon (POC, estimated from hyperspectral absorbance and attenuation) and variable to maximum fluorescence (F_v/F_m), were measured from water collected 6.7 m below the surface, from the ship's underway seawater system. Hyperspectral absorbance and attenuation were measured as part of a complementary effort to model primary productivity in the Ross Sea (White et al., 2014; White et al., in preparation, absorbance data not shown here). For attenuation and particulate carbon, this source water was routed through a Vortex debubbler and a valve control device that automatically diverted the inflow to a PALL Supor 0.2 μm membrane filter for the first 10 min of every hour prior to passing through a Wetlabs hyperspectral absorbance and attenuation (ac-s) meter. For the remaining 50 min of each hour, the valve control device routed water from the debubbler directly to the ac-s. Particulate beam attenuation spectra were corrected as per Slade et al. (2010). All raw data were binned to 1 min intervals, the dissolved signal [$c_d(\lambda)$] was subtracted from the unfiltered signal [$c_t(\lambda)$] to obtain particulate spectra [$c_p(\lambda)$] which were then corrected for variations in particle beam attenuation resulting from residual temperature differences between filtered and unfiltered spectra (see Slade et al. (2010)). For reference, at 660 nm the magnitude of dissolved attenuation values were $0.0220 \pm 0.0138\ m^{-1}$. Discrete samples (triplicate samples collected at 6 discrete times, $n=18$) were collected from the outflow of the ac-s for calibration of $c_p(660)$ to particulate organic carbon (POC) as measured by high temperature combustion of particulate matter filtered onto glass fiber filters. The POC to c_p slope for this data set is 345 mg C m^{-2} with an intercept of 1.7 mg C m^{-3}; these values are used to transform the full corrected $c_p(660)$ dataset to POC values. This slope is consistent with that reported by Cetinić et al. (2012) for diatom dominated communities within the mixed layer (369 ± 23 mg C m^{-2}) and with the global analysis of Gardner et al. (2006) which report a slope of 381 ± 3 mg C m^{-2} and an intercept of 9.4 ± 0.6 mg C m^{-3}. For reference, we have also compared $c_p(660)$ to the attenuation coefficient obtained from a shipboard beam transmissometer ($-\log10\,(T)$) although the latter was connected to a different flow through seawater inlet.

Chlorophyll *a* fluorescence was measured using a Satlantic FIRE fluorometer (Gorbunov and Falkowski, 2004) and the ratio of variable to maximum fluorescence (F_v/F_m) was calculated from F_o and F_m. A reference excitation profile was collected during the cruise using rhodamine dye as a standard. F_v/F_m was measured with a single turnover 80 μs flash (peak emission 455 nm) followed by a 20 ms multiple turnover flash. Ten repetitive samples were averaged for calculation of F_o and F_m using the software provided by the manufacturer. Blank F_v/F_m values were generated daily from filtered (0.2 μm syringe filter) seawater to correct F_o and F_m values prior to

calculation of F_v/F_m. Blank values were 5–10% of sample values. Underway variable to maximum fluorescence along two transects across Pennell Bank (Fig. 1), from the 400 m isobath towards the southeast, was used as a proxy for Fe status. Data were binned according to their nearest proximity to one of 11 points from stations 16/24/41 to 28 across the central Pennell Bank transect (Fig. 1B); points were 12 km apart on this 120 km transect (not shown). Similarly, data were binned according to their nearest proximity to one of eleven points from stations 50 and 46 across the northern Pennell Bank transect (Fig. 1B); points were 13.6 km apart on this 136 km transect (not shown). To minimize the effects of photo-bleaching, observations corresponding to mast PAR values greater than 300 μmol photons m^{-2} s^{-1} were omitted (as described below, this translates to an approximate irradiance of 100 μmol photons m^{-2} s^{-1} at the collection depth). Due to instrumentation problems, F_v/F_m measurements were not available for the entire cruise. Data were compiled from four passages across the central transect and one across the northern transect.

2.3. Process casts and discrete sample collection

Vertical profiles were obtained with a Sea-Bird 911+ CTD equipped with WetLabs FLRTD fluorometer, Biospherical Instruments QSP-2300 PAR sensor, and a SeaBird SBE 43 oxygen sensor. Mixed layer depth (MLD) was determined as that where sigma-*t* increased by 0.125 kg m^{-3} (10 dbar reference; Lorbacher et al. (2006); Supplemental Table 2). For comparison, depths were also calculated using two other methods (based on O_2, Castro-Morales and Kaiser (2012); on a σ_θ difference of 0.03 kg m^{-3}, De Boyer Montégut et al. (2004), both with a 10 m reference). These shallow environments are subject to significant tidal activity (Kohut et al., 2013) so we tested whether there might be a relationship between mixed layer depth and diurnal tidal phase; no such relationship was evident (Supplemental Table 2, Supplemental Figs. 2 and 3). The median MLD for each station visit was used in all subsequent calculations. Stations 61 and 64 were assumed to represent a single location, since the elapsed time between the casts at these stations (0.36 d) was comparable to times between individual casts at a single station.

Discrete macronutrient samples, including nitrite+nitrate (hereafter nitrate) and silicate, as well as particulate organic carbon (POC), particulate organic nitrogen (PON) and chl *a* samples were taken from 0 to 200 m. Samples were filtered for chlorophyll on 25 mm GF/F (Whatman) filters and frozen (−80 °C) until extraction in acetone. Extracts were measured on a Turner Trilogy fluorometer, calibrated using the extinction coefficients of Porra et al. (1989).

2.4. Dissolved Fe concentrations

Seawater samples were collected for Fe analysis and incubations from stations 7 and 61 (CPB), 16, 24 and 41 (WF) and 48 (NPB; Fig. 1B). In addition, samples were collected from a station just beyond the shelf break (St. 14, 72° 34.98′ S, 178° 30′ E, $z=1887$ m) at 450 m for Fe analysis and an incubation treatment. Samples were collected using a trace-metal clean sampling system with 12 L Teflon lined GO-FLO (General Oceanics) bottles, and filtered subsamples were drawn into acid pre-washed 125 ml polymethylpentene bottles after three sample rinses (Measures et al., 2008). Samples were stored in polyethylene bags in the dark at room temperature before Fe determination, which was usually within 24 h of collection. Duplicate samples were collected for shore-based determination of dissolved Fe by Inductively Coupled Plasma Mass Spectrometry (ICP-MS). Shipboard Fe samples were acidified (125 μl sub-boiling distilled 6 N HCl), microwaved for 3 min in a 900 W oven to achieve a temperature of 60 ± 10 °C, and cooled for at least 1 h prior to Flow Injection Analysis (FIA; Measures et al. (1995)). A 3 min pre-concentration of sample (~9 mL) onto an 8-hydroxyquinoline resin column yielded a detection limit of 0.02 nM and a precision of 3.6% at 0.20 nM. Shipboard FIA data were initially corrected for the system and reagent blanks using a sample spiked with EDTA. We have found however that this correction does not always provide a completely accurate assessment of the blank and thus undertake a separate assessment of the blank by running a subset of samples by shore-based ICP MS. The results of these shore-based determinations are then regressed against the shipboard values yielding a more accurate assessment of the blank which is then used to correct the shipboard values (Hatta et al., 2013, 2015; Milne et al., 2010). For shore based ICP MS determinations, acidified samples (12–15 mL, 0.024 M HCl) were spiked with ^{57}Fe (91.9% ^{57}Fe, 7.2% ^{56}Fe), pre-concentrated with an in-line micro-column containing ~200 μL of Toyopearl AF Chelate-650 resin, and extracted in sub-boiled 1 M trace metal clean nitric acid. The eluates were analyzed on an ICP-MS (Thermo Scientific, Element 2, Medium-Resolution) with Apex-Q high efficiency inlet system (Elemental Scientific) and a self-aspirating nebulizer (PFA, Elemental Scientific) at 400 μL min^{-1}. The ICP-MS detection limit for Fe (0.01 ± 0.01 nM) was calculated from 3 standard deviations of replicate measurements of the acid blank. ICP MS determination of Fe in the GEOTRACES open ocean reference material yielded 0.960 ± 0.057 nM, in good agreement with the inter-laboratory averages of 1.00 ± 0.10 nM reported for these materials (consensus value by Bruland, May 2013).

Water masses were identified as MCDW according to the three criteria (Jacobs and Giulivi, 1998; Orsi and Wiederwohl, 2009). There must be a local maximum in temperature at depth which corresponds to a local dissolved O_2 minimum. These features must also fall within the neutral density boundaries (28–28.27). CDW at station 14 was identified as that at 300–600 m with a thermal maximum (1.35 °C, slightly cooler than the canonical 1.5 °C threshold) and O_2 minimum. It is important to realize that the original MCDW derived from CDW enters the Ross Sea and becomes increasingly modified by mixing processes on the shelf with the waters above and below it, thus the original signatures of this water mass become successively eroded. The comparison of deep water dissolved Fe concentrations on Pennell Bank to those in MCDW to gauge the latter's importance as an Fe source was complicated by the eroded T, O_2 and neutral density signatures of MCDW on Pennell Bank. Nonetheless, to get a general idea of the potential role of MCDW on Pennell Bank deep water Fe content, the average Fe concentration from 100 to 200 m at each station was calculated from measured values at discrete depths by trapezoidal integration, using midpoint Reimann sums.

2.5. Shipboard Fe manipulation experiments

All materials were cleaned and pre-conditioned to minimized trace metal contamination as described previously (Kustka et al., 2015). Trace metal clean seawater was collected as detailed above and bottles were removed from the rosette and carried into a trace-metal clean van for subsequent processing. GO FLOs were emptied into cleaned 20 L polycarbonate carboys with C-flex tubing (Cole-Parmer), which were transported to a HEPA workstation inside a HEPA filtered “bubble” room, where ~8 L aliquots were dispensed into cubitainers.

2.6. Addition of micronutrients and deep waters

Ferric chloride, from a 100 μM stock in 1 mM Q-HCl, was added to achieve a final concentration of 1 nM Fe. Deep water (of varying characteristics and sources, described below) was added to provide a 20% contribution to the total volume. Deep water collected

for incubations at stations 16 and 24 had marked MCDW characteristics but those at stations 7 or 61 did not (see below). In addition, CDW was collected from station 14 on Julian day 26.13 and used in an incubation with surface water from station 16 to contrast the effects of CDW and MCDW. Cubitainers were incubated within a van maintained at 1–2 °C and equipped with spectrally corrected blue light. Irradiance in the center of a cubitainer was ~40 μmol photons m^{-2} s^{-1}.

MCDW collected for incubation experiments fit the criteria specified above (neutral density, local maxima and minima in temperature and dissolved O_2, respectively). The O_2 sensor on the trace metal rosette was subject to periodic freezing on deck (the process rosette was protected) and the dissolved O_2 profiles from the trace metal rosette were useful to define O_2 minima but were qualitative. O_2 profiles from process casts taken before or after trace metal casts verify the depths of these O_2 minima.

2.7. Phytoplankton response to Fe and deep water additions

Four metrics (two estimates for growth rate, Si:N removal ratio, and variable to maximum fluorescence, F_v/F_m) were measured over the course of incubations, about every 3 days for 9 days (or for 6 days in the case of station 48) to assess the relative Fe status of phytoplankton. Phytoplankton growth rates were estimated based on chl *a* accumulations and decreases in nitrate concentrations during the experiments. Variable to maximum fluorescence was measured at each sampling event to indicate physiological stress from iron limitation. Silicate to nitrate removal ratios were also calculated based on nutrient levels at the start and end of each experiment. Samples were filtered for chlorophyll on 25 mm GF/F (Whatman) filters and frozen (−80 °C) until extraction in methanol. Extracts were measured on a Turner AU-10 fluorometer, calibrated using the extinction coefficients of Porra et al. (1989). To measure variable to maximum fluorescence, samples were acclimated at 1–2 °C in darkness for 20 min prior to measurement. Due to instrument problems, active fluorescence measurements were not available from cast samples at station 7. Underway variable to maximum fluorescence values were 0.264 ± 0.021 at this location 19 and 22 days later.

Nitrate and silicate concentrations were analyzed on-board using a five-channel Lachat Instruments QuikChem FIA system (Armstrong et al., 1967; Atlas et al., 1971). Minimum detection limits for nitrate and silicate throughout the cruise ranged from 0.148 to 0.201 μM and from 0.58 to 1.76 μM, respectively. Silicate: nitrate removal ratios were calculated from the ratio of the differences between the beginning and end of incubations (Supplemental Table 3). Chl *a* based growth rates were calculated as the slope of the natural log of chlorophyll concentration versus time from time zero. For nitrate removal -based growth rates, we assumed removal was partitioned into particulate organic nitrogen (PON). PON at time zero was estimated from the median mixed layer PON, and growth rates were calculated as the natural log of PON accumulation through time.

Responses of each of the metrics to various treatments were evaluated with a single classification analysis of variance with planned contrasts. Hypotheses tested included whether (1) phytoplankton growth rates were Fe-limited (as evidenced by a stimulation in growth as a result of ferric chloride additions, compared to no Fe added controls, for stations 7, 16, 24 and 48), (2) whether additions of filtered MCDW (stations 16 and 24) or filtered deep water (station 7) stimulated growth relative to control conditions, and (3) whether additions of unfiltered MCDW stimulated growth. This was done for station 24, by comparing unfiltered MCDW responses to control conditions. From each set of treatments, the threshold value for significance was calculated for each experiment as α/k, where $\alpha=0.05$ and k indicates the number of comparisons made within each treatment ($k=2$, 3, 3, and 1 for incubations from station 7, 16, 24 and 48, respectively). As a result, Bonferroni corrected α' values for these (one-tailed) comparisons were 0.025, 0.0167, 0.0167 and 0.05, respectively.

2.8. Photosynthesis-irradiance relationships and in situ Fe demand

Photosynthesis-irradiance experiments were conducted using a ^{14}C-radiotracer method. Samples were collected from 5 m using the trace metal clean rosette or by TMC pumping of surface water (Vink et al., 2000). Water samples were processed in a flow hood and all plastic ware was acid washed with 10% trace metal grade HCl (Martin et al., 1991). Incubation chambers consisted of two photosynthetrons (OHPT Inc. Delaware, USA); irradiance was controlled with both copper sulfate and neutral density filters with incubation light levels ranging from 0 to 500 μmol photons m^{-2} s^{-1}. Incubation temperatures were maintained at a constant 0 °C via circulating water baths filled with a 90% glycerol solution. At each station 50 μL of a 0.2 mCi ^{14}C bicarbonate stock was added to 80 mL of sample to achieve a final ^{14}C-concentration of 125 pCi mL^{-1}. Following the addition, the sample was gently inverted and 100 μL placed into a scintillation vial containing 1 mL of 0.2 μm filtered seawater (FSW) and 100 μL of β-phenethylamine to determine the specific activity. The remaining sample was dispensed among 15 polyethylene scintillation vials with a final volume of 5 mL per vial. Samples were incubated for 24 h (and therefore reflect net primary production rather than gross production which is often seen in shorter incubations (Halsey et al., 2011) and acidified with 250 μL of 10% hydrochloric acid in a fume hood for 8–12 h, after which 19 mL of Ecolume scintillation fluid were added. Radioactivity was measured on Tri-Carb liquid scintillation counter after 24 h and again after 1 week. For each experiment, duplicate vials were wrapped with aluminium foil before incubation and the corresponding dark ^{14}C-fixation was subtracted from the light values. Primary productivity was calculated by multiplying the percent of carbon labeled by the total carbon available for photosynthesis (e.g. total alkalinity calculated from SST and salinity measured at each station as per Lee et al. (2006)) and dividing by incubation time. All rates were normalized to chlorophyll *a* concentrations. The results of each P–E experiment were fitted to a hyperbolic tangent model using least-squares non-linear regression in Matlab™.

Depth and diel integrated water column net productivity was determined from the photosynthesis-irradiance relationships described above, the empirical relationship between above-sea PAR and time of day determined during this sampling campaign (Eq. (1))

$$PAR = 410^{*} \sin(2\pi/24^{*}(GMT + 4.71\ h) + 459. \quad (1)$$

the transmission of PAR into the ocean and the light attenuation coefficients calculated within the mixed layer at each station. The transmission of PAR into the ocean was determined at one hour intervals over a 24 h period using the solar zenith values (at Julian day 32 and at 74.5° S) and a cruise-averaged wind speed of 7.4 m s^{-1}, following Walsby (1997). This resulted in transmission values ranging from 56% to 80% of surface (mast) PAR, depending on time of day.

At each station, the hourly irradiance at each meter in the mixed layer was calculated from ambient PAR, PAR transmission into the surface ocean and the light attenuation coefficient. Hourly net C-fixation at each depth was determined from this irradiance, the measured P–E relationship, and chlorophyll content. Productivity was calculated for subsequent 5 m depths beneath the mixed layer (until reaching the 1% light level), using the depth averaged chl *a* content, light at mid-depth for that stratum, and the P–E relationship. These data were integrated over 24 h to obtain new production (mol C m^{-2} d^{-1}).

Table 1
Station locations and characteristics. Station sampling times, station region (CPB, Central Pennell Bank; NPB, Northern Pennell Bank; WF, western flank), and latitude and longitude are reported. Median mixed layer depth, mixed layer averaged chlorophyll *a*, vertical extinction coefficients (k), and total water depth (Z) were determined from process casts. Further details, including all mixed layer determinations at these locations, are found in Supplemental Table 2.

Julian day	Station	Region	Lat	Lon	MLD (m)	chl *a* ($\mu g\ L^{-1}$)	k (m^{-1})	Z (m)
22.8–23.2	7	CPB	−74.502	178	30	4.67	0.226	275
27.1–27.3	16	WF	−74.133	176.666	30	0.51	0.053	385
31.7–32.2	24	WF	−74.133	176.666	29.5	1.00	0.085	395
37.1–37.2	41	WF	−74.133	176.666	32	0.64	0.081	402
38.2–38.5	48	NPB	−74.201	178.753	27	0.75	0.084	260
40.9-41.3	61/64	CPB	−74.5	178	35	3.37	0.210	276

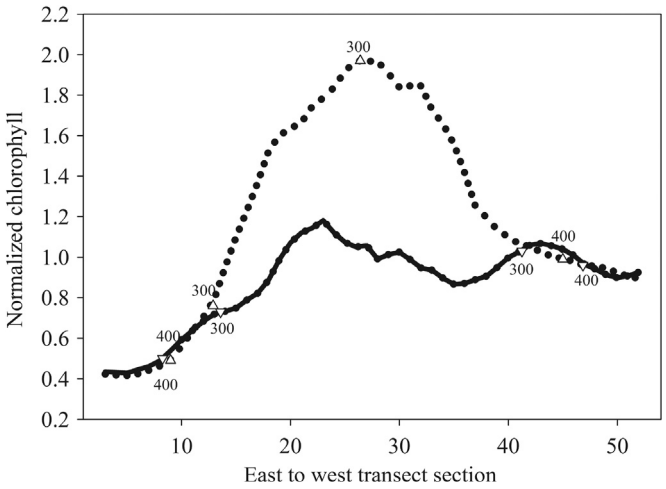

Fig. 3. Mid-summer MODIS-derived chlorophyll *a* across two Pennell Bank transects over a six year period. The northern and central transects (see also Fig. 1 B) are indicated in solid and dashed lines. The location of isobaths (300 and 400 m) across the northern and central transects are indicated with triangles and inverted triangles, respectively. All data were normalized to the overall average from these transects. Running averages over 5 sections (along 54 sections from east to west, as described in methods), are presented for clarity.

Using regionally averaged surface PAR values minimized confounding factors of station location and short term variability in irradiance due to cloud cover. Similarly, irradiance penetrating into the surface ocean was estimated to avoid artifacts of ship shading or deck lighting of the PAR sensor on the CTD rosette.

The Fe demand at each station was estimated from net productivity, euphotic zone integrated phytoplankton biomass, and the calculated Fe:C ratio. The Fe:C ratio of surface phytoplankton was estimated from upper water column Fe removal, normalized to N. For each nutrient, surface and subsurface pools were estimated by trapezoidal integration from 0 to 100 m and 100 to 200 m. While the mixed layers were always <100 m, these two layers were chosen to represent the proximal Fe supply because the steepest segments of the ferricline started to relax near 100 m, with relatively low and uniform surface water concentrations. The sub-surface pool supplying the upper 100 m was assumed to extend from 100 to 200 m (rather than to the bottom), because the relative horizontal and vertical transport of deeper waters (and therefore their potential contribution to surface waters) is not clear. For integration, values obtained at the shallowest depth sampled (20–38 m) were assumed to extend to the surface. For each station, an estimate of the Fe:C ratio was calculated from the Fe:N removal ratio within the upper 100 m and an assumed C:N molar stoichiometry of 6.37 for Ross Sea diatoms (Arrigo et al., 1999). Fe:C values for WF and CPB regions were calculated from average values calculated from each station ($n=3$ and 2, respectively); the NPB region was visited once (station 48). The use of dissolved nutrient profiles to estimate Fe:C quota can be complicated by Fe supplied to these surface waters from ice melt. Sea ice derived iron can be sequestered shortly after spring-time ice melting events (Sedwick and DiTullio, 1997; Sedwick et al., 2011), which would lead to an underestimate of the true Fe:N quota. We cannot quantify the effect this may have had during our field campaign, but this may have been negligible since an analysis of gridded monthly average sea ice concentration (SMMIS) shows the polynya opened early and to a larger extent than in the preceding and following years (data not shown).

At each station euphotic zone Fe demand for new C production was estimated based on the integrated C production and the Fe:C ratio. The vertical mixing ($m\ d^{-1}$) required to deliver the dissolved Fe to meet this demand to the euphotic zone (assuming 100% of this is met by this source) was estimated by dividing the Fe demand ($mol\ m^{-2}\ d^{-1}$) by the integrated dissolved Fe concentration in the 100–200 m layer ($mol\ m^{-3}$). This subsurface layer was chosen, rather than the entire sub-euphotic zone, for the reasons mentioned above.

2.9. Water column physics and optics from glider AUV sections

A deep Slocum electric glider (Teledyne Webb Research) was deployed to sample between 10 m below the surface and 10 m above the bottom and was equipped with a sensor suite that characterized physical structure (conductivity, temperature, depth, dissolved O_2), in situ fluorescence and optical backscatter. On December 10, 2010 the deep glider was deployed from the sea ice edge near Ross Island. The 52 d mission took the glider east along 76.5° S before turning toward the northwest toward Pennell Bank. Once the ship started its survey on January 20th, 2011, the complementary glider sampling provided high vertical and horizontal resolution of the physical characteristics in the vicinity of the flow along western Pennell Bank and into Joides Trough. The glider data discussed in this analysis was focused on the portion of the mission conducted over the western flank of Pennell Bank (Fig. 2). Over this segment of its mission, the glider transited northeast toward WF, turned southeast and continued to the CPB region. The data resolution was 0.25 m (vertical) and ~2.2 times the water depth (horizontal). Data were verified during calibration casts with the glider secured to the ship's rosette.

The physical supply rates of deep water to the surface layer over Pennell Bank were estimated from a Regional Ocean Modeling System (ROMS; Haidvogel et al. (2008) and Shchepetkin and McWilliams (2009)) 3-D model simulation of the Ross Sea. The model domain includes all of the Ross Sea continental shelf (including the cavity underneath the Ross Ice Shelf) and extends north to 67.5° S. Horizontal grid spacing is 5 km and there are 24 vertical layers. The model not only includes a dynamic sea-ice model (Budgell, 2005), but also simulates the mechanical and thermodynamic interactions between the Ross Ice Shelf and the waters underneath (Holland and Jenkins, 1999; Dinniman et al., 2011). This study uses a model run covering the time period 15 September 2010 to 27 February 2012 and is forced with six hourly,

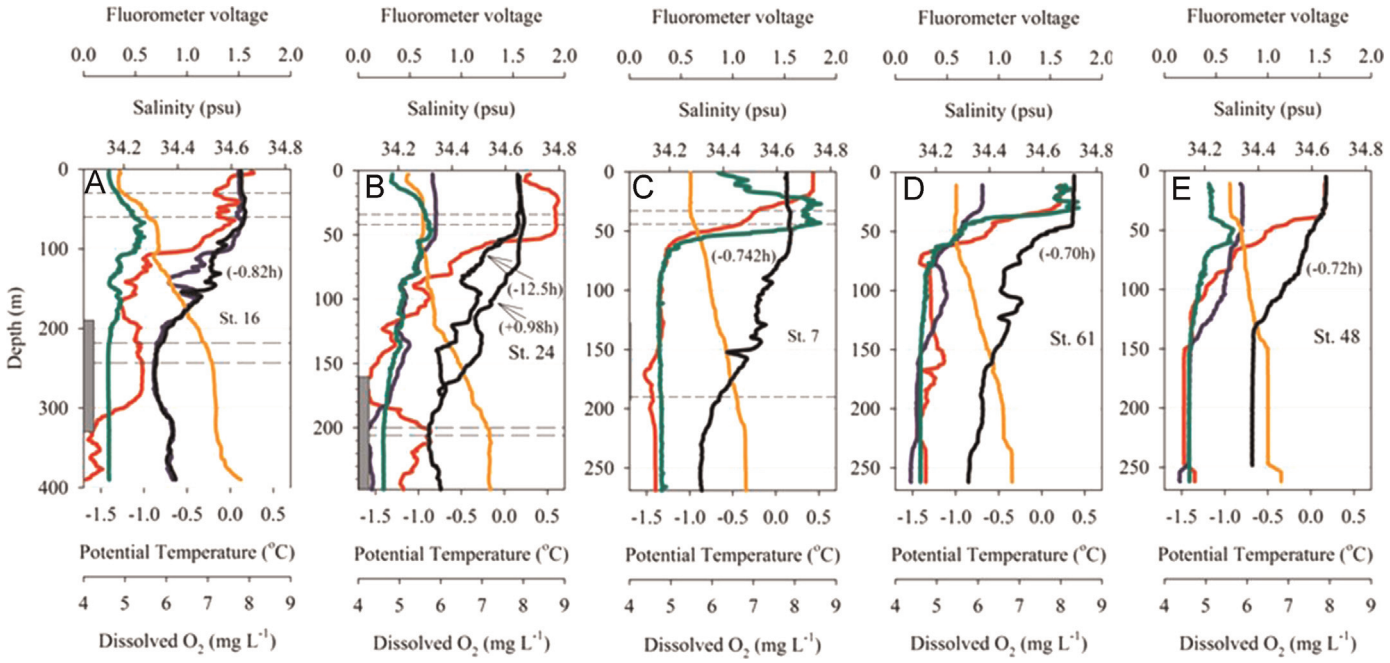

Fig. 4. Vertical profiles of temperature (red), salinity (orange), dissolved oxygen (blue and black, described below) and chlorophyll a fluorescence (green) from trace metal casts used for incubations. Stations 16 and 24 (Panels A and B) have characteristics indicating the presence of MCDW (potential density 28–28.27 coincident with local temperature maxima and oxygen minima, indicated with shaded bars on *y* axes), while these characteristics at stations 7, 61 and 48 (Panels C–E) have been eroded by further mixing. Shallow and deep water sources for incubations (stations 7, 16 and 24 only) are indicated by dashed lines. The O_2 sensor on the trace metal rosette was subject to periodic freezing on-deck (values shown in blue), but the sensor was protected for the 'process cast' rosette (values shown in black). The process cast times relative to trace metal casts are shown in parentheses. (For interpretation of the references to color in this figure legend, the reader is referred to the web version of this article.)

0.75° horizontal resolution, European Centre for Medium-Range Weather Forecasts (ECMWF)-Interim reanalysis winds and atmospheric temperatures (Dee et al., 2011), with the rest of the atmospheric forcing fields (air pressure, humidity and clouds) being the same as in Dinniman et al. (2007). There is no surface relaxation of temperature or salinity. Tidal forcing at the lateral boundaries is from the CATS2008 tidal model, which is an updated version of the inverse tidal model of Padman et al. (2002). Further details on this particular model setup can be found in Marsay et al. (2014).

Throughout the simulation we used virtual dye and the trajectories of neutrally buoyant passive particles to estimate physical delivery rates of CDW and deep water to different regions of the bank. At the start of the simulation, an artificial dye tracer with an initial concentration of 100.0 representing CDW is placed in water off the continental shelf (defined by the 1200 m isobath) at all depths where the temperature is greater than 0.0 °C. This tracer is then allowed to advect and diffuse freely over the entire model domain in order to track pathways of CDW onto the shelf (Dinniman et al., 2011). There is no surface or bottom flux of the CDW tracer, but there is a lateral source at any off shelf boundaries where the boundary information meets the criteria for CDW. Changes in dye concentration among the different water masses along these trajectories quantified the vertical supply of these deep waters into the upper water column. The particles are advected by having the rate of change of the position of the particle at every model time step be equal to the three dimensional advective velocity of the model (at the time and position of the tracer particle) plus a vertical diffusion term which was included by adding a random walk in the vertical direction (Hunter et al., 1993; Visser, 1997). Particles were initialized over Pennell Bank within the 500 m isobath on a fixed initial grid. This grid was 15 km in the horizontal layered every 20 m in the vertical starting 5 m below the surface. Drifters on this grid were released 8 times, 5 days apart, beginning at 00:00 Z on January 13, 2011. The last release was on February 17, 2011 and each drifter was tracked until the end of the model (1 year later). The releases overlap with the shipboard sampling and resolve spring/neap tidal variability. For each particle we recorded the hourly model estimates of temperature, salinity, density and dye concentration along its trajectory.

The dye was used to track the intrusion and subsequent mixing of CDW into waters within our study area. Over the course of the simulation, dye concentrations at each drifter location documented the propagation of dye (MCDW) onto the Ross Shelf. Dye concentrations were recorded at each simulated drifter location over time within regions of the bank (the western flanking, eastern flanking, central Pennell Bank, and northern Pennell Bank, respectively), represented by our sampling stations (Fig. 6). The average dye concentrations for all drifters within each region were used to estimate a time series of dye concentration. The rate of change of the dye concentration in surface waters (0–100 m) at each station relative to the dye concentrations in the layer below (100–200 m) was used to estimate the physical delivery rate of the dye to the surface waters over that region of the bank, and was calculated in two ways. First, the slope of surface water dye concentration over time (65 days) was divided by the median deep water dye concentration. Second, the median surface water increase in dye concentration (deep water normalized) was calculated, as follows. The daily increases in dye concentration ($n=64$) were calculated and divided by the deep water dye concentration at each time step (averaged over two days). The median value was determined from this population of values. Data from the first and second methods are presented here as, "65 day integrated" and "median daily" values, respectively.

To better determine the potential sources of upwelled waters, the locations of drifters observed in surface waters at station CPB or NPB (10 km radius) on either 31 Jan or 14 Feb were hindcast 14 days. Together these data were used to evaluate whether the vertical supply of deep waters could satisfy the Fe demands to

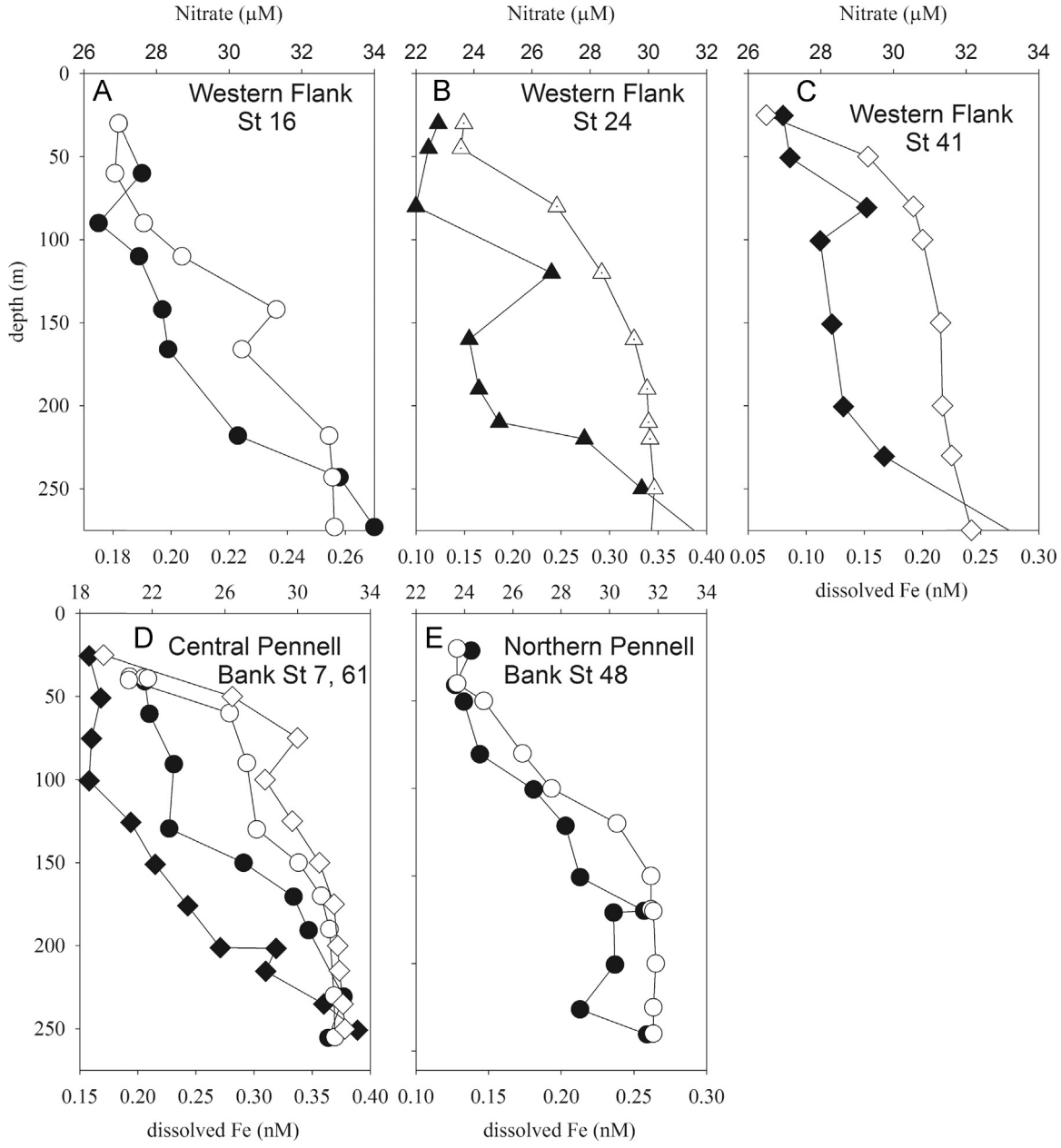

Fig. 5. Dissolved Fe and nitrate depth profiles. Filled and open symbols represent Fe and nitrate, respectively. (A–C) dFe profiles from western flank stations 16, 24 and 41. (D) dFe profiles from central Pennell Bank stations 7 (circles) and 61 (diamonds). (E) dFe profile from northern Pennell Bank station 48.

support the measured rates of productivity at the WF, CPB and NPB regions.

3. Results

During this sampling campaign, both underway estimates of particulate organic carbon and satellite/shipboard chlorophyll *a* reveal elevated biomass in the central region of Pennell Bank (CPB; Fig. 1B, Table 1) relative to adjacent waters at the western flanking (WF) and northern Pennell Bank (NPB) regions. Station 7 had the highest chl *a* levels (4.67 μg chl *a* L^{-1} within a 30 m ML), and chl *a* at station 61/64 (18 days later) was ~3.37 μg chl *a* L^{-1} in a 35 m ML, comparable ML-integrated chl *a* values. Station 48 (NPB) had a chl *a* concentration of 0.75 μg L^{-1}, comparable to values of 0.72 ± 0.25 μg L^{-1} at WF stations. These observations are consistent with the glider profiles which show dramatic increases in chl *a* from Joides Trough into the CPB region (Fig. 2B). MODIS data suggest the high chl *a* observed at stations 7 and 61/64 during this study is a recurring feature during the summer months (Fig. 3, Supplemental Fig. 1, and Supplemental Table 1). Along the CPB portion of the transect, chl *a* levels were ~4 times greater than those observed in WF region waters, and about twice as high as levels seen in the transect 95 km to the north.

The MCDW feature along the WF region was persistent throughout repeated station visits (Fig. 4A and B, other data not shown). At central Pennell Bank (CPB) stations 7 and 61/64 and northern Pennell Bank (NPB) station 48, all in shallow (< 300 m) waters, the MCDW signatures were eroded, as might be expected based on mixing with shelf waters as it follows the counter-clockwise pathway around the bank (Kohut et al., 2013).

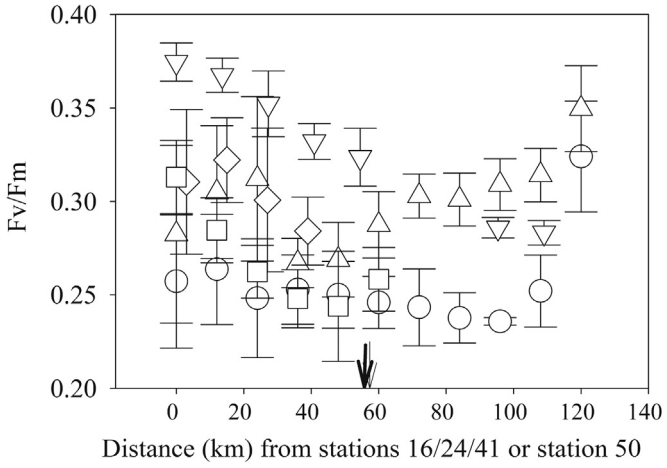

Fig. 6. Variable to maximum fluorescence along Pennell Bank transects. Distances are calculated along transects shown in Fig. 1B relative to stations 16/24/41 or station 50. Average underway values along the CPB transect during Julian days 32, 37, 40 and 41 are represented by circles, triangles, diamonds, and squares, respectively, while values along the NPB transect (Julian day 37 and 38) are represented by inverted triangles. Error bars represent standard deviations. Julian day 40 observations are offset by +3 km for clarity of presentation. Bold and regular arrows indicate locations of station 7 and 48 along transects.

3.1. Dissolved Fe profiles and in situ Fe status

Depth-integrated dissolved Fe within MCDW water masses from three WF stations (17 total measurements) averaged 0.233 nM (± 0.019 nM, n=3; Fig. 5). These were lower than the 0.46 nM observed in the CDW source off the shelf, and comparable to the 0.240 ± 0.039 nM observed at 100–200 m within the relatively shallow CPB and NPB regions. At all stations, vertical profiles of dissolved Fe exhibited characteristic nutrient behavior, with lower concentrations in the upper 100 m, ranging from 0.12 to 0.21 nM (Fig. 5). Variable to maximum fluorescence across CPB and NPB transects reveal little consistent spatial variability (Fig. 6), with transect averages ranging from ~0.24 to ~0.37 suggesting widespread limitation. It is worth noting that this proxy for Fe status is subject to variability due to taxonomic composition (Suggett et al., 2009).

Fe additions in incubations led to dramatic increases in chl *a* (Fig. 7), yielding net growth rates of ~0.26–0.37 d^{-1} (Table 2). The chl *a*-based growth rates in controls were 31–44% of growth rates obtained with Fe addition, while growth rate estimates based on nitrate removal in controls were 43–56% of those with Fe additions. Average growth rates based on nitrate were, on average, 80% of those based on chlorophyll.This difference may reflect deviations from the assumption that the *in situ* PON concentrations approximate that of ambient phytoplankton and that all phytoplankton growth is fueled by nitrate uptake (discounting the role of recycling of other nitrogenous substrates). Nonetheless, these and other metrics allowed us to evaluate the responses towards Fe and various deep water additions. Iron additions also led to increases in variable to maximum fluorescence (from 0.158 to 0.503 for station 16, from 0.213 to 0.565 for station 24, and from 0.332 to 0.541 for station 48, with the coefficient of variation between replicate cubitainers less than 2%). Iron addition at station 7 resulted in an average F_v/F_m value of 0.373 after 9 d of incubation, greater than that obtained in control treatments (0.221), and the average value observed at or near this location later in the cruise (0.263). These additions also led to decreases in Si:N removal ratios, to 1.28 ± 0.08, 1.27 ± 0.05, 1.05 ± 0.30 and 0.97 ± 0.10 mol:mol for stations 7, 16, 24 and 48 respectively, some 34–56% of control values. For all incubations and metrics, the responses to iron additions were significant compared to control treatments (Supplemental Table 4).

Filtered deep water additions did not have a consistent effect on any of these four metrics. Only deep water additions at station 7 elicited a modest effect on nitrate based growth rates (0.130 ± 0.0014 versus 0.085 ± 0.020 for no iron controls; p = 0.018, $\alpha^{/}$=0.025).. The lack of a consistent effect from deep water addition for this incubation experiment at this station is consistent with the small final concentration of Fe added from deep water (0.028 nM; Table 2).Station 24 incubations amended with unfiltered MCDW had significantly lower Si:N removal ratios(p= 0.014, $\alpha^{/}$=0.0167; Figure 8, Supplemental Table 4) and nitrate-based growth rates (p=0.014, $\alpha^{/}$=0.0167; Table 2, Supplemental Table 4), but there was no differential responses for the other metrics to this treatment.. The source water for this incubation contained about ~1 nM particulate labile Fe (Lam et al., 2014), which would have raised the Fe inventory by an additional 0.2 nM (Table 2).

Stations from WF and NPB regions exhibited chl *a*-specific maximum rates of photosynthesis (P^b_{max}) of 1.68 ± 0.13 g C g chl a^{-1} h^{-1} (n=4). In contrast, CPB stations 7 and 64 (Julian days 22–23 and 40–41) had P^b_{max} values of 4.21 ± 0.4 and 3.20 ± 0.29 g C g chl a^{-1} h^{-1}, respectively (Table 3). Areal productivity at CPB stations (457 and 300 mmol C m^{-2} d^{-1} for stations 7 and 61/64, respectively) was, on average, ~4.5-fold higher than surrounding stations at WF and NPB (Table 3).

Estimates of Fe:C demand, based on Fe and nitrate deficits in the upper 100 m, did not show any apparent spatial trends, with values ranging from 0.8 to 2.5 μmol:mol Fe:C among stations. Average Fe:C ratios at each location (from multiple station visits and profiles) ranged from 1.5 to 2.1 μmol:mol. These average Fe:C demands (alternatively, an assumed phytoplankton Fe:C ratio of 7 μmol:mol) were multiplied by the net primary production at each station to calculate areal Fe demands (nmol Fe m^{-2} d^{-1}). These calculated demands ranged from ~790 to 3200 nmol Fe m^{-2} d^{-1} at station 7 and 520–2100 nmol Fe m^{-2} d^{-1} 18 days later (at station 61/64). The calculated lower and upper ranges for the Fe demand in the WF region were ~80–160 and ~390–740 nmol Fe m^{-2} d^{-1}, while station 48 (NPB) had an Fe demand from 190 to 640 nmol Fe $m^{-2}d^{-1}$. Assuming Fe is supplied solely by vertical supply requires a velocity of 2.4–11.2 m d^{-1} (at CPB stations) and of ~0.7–4.0 m d^{-1} at other stations (Table 3).

The quantification of CDW-derived dye from the model revealed spatiotemporal patterns in dye concentrations consistent with the counter clockwise circulation of deep water around and across Pennell Bank (Kohut et al., 2013). In the western region, dye in the three deepest layers was present at approximately equal concentrations (~0.35 of CDW) and did not increase over this time (Supplemental Fig. 4A). These are consistent with the barotropic flow in the region and also suggest these deep water had achieved steady state with respect to dye input and removal. Dye content from 0 to 100 m decreased slightly over time, resulting in a calculated negative supply rate (−0.30 to −0.37 m d^{-1}; Table 4). In the CPB, dye increased in deep waters (> 100 m) from ~13.5% to 21%, showing equilibrium conditions had not yet been reached. The presence of the CDW tagged dye at CPB indicates that these deep waters are derived in part by MCDW. The estimated vertical supply ranged from 0.18 to 0.43 m d^{-1}, depending on the method of calculation (Table 4). Trajectories of particles within 10 km of our sampling stations identified differences in potential source water. Over the Central Pennell bank station, 14 day trajectories from deeper waters originated from the southwest, within the vicinity of the 300 m isobaths (Fig. 9). In contrast, just 95 km to the north (station 48; NPB), particles in the upper 100 m were primarily derived from upper water sources from the north. This suggests complex circulation patterns that may play a role in the observed disparities in historical chlorophyll levels along these two transects (Fig. 3).

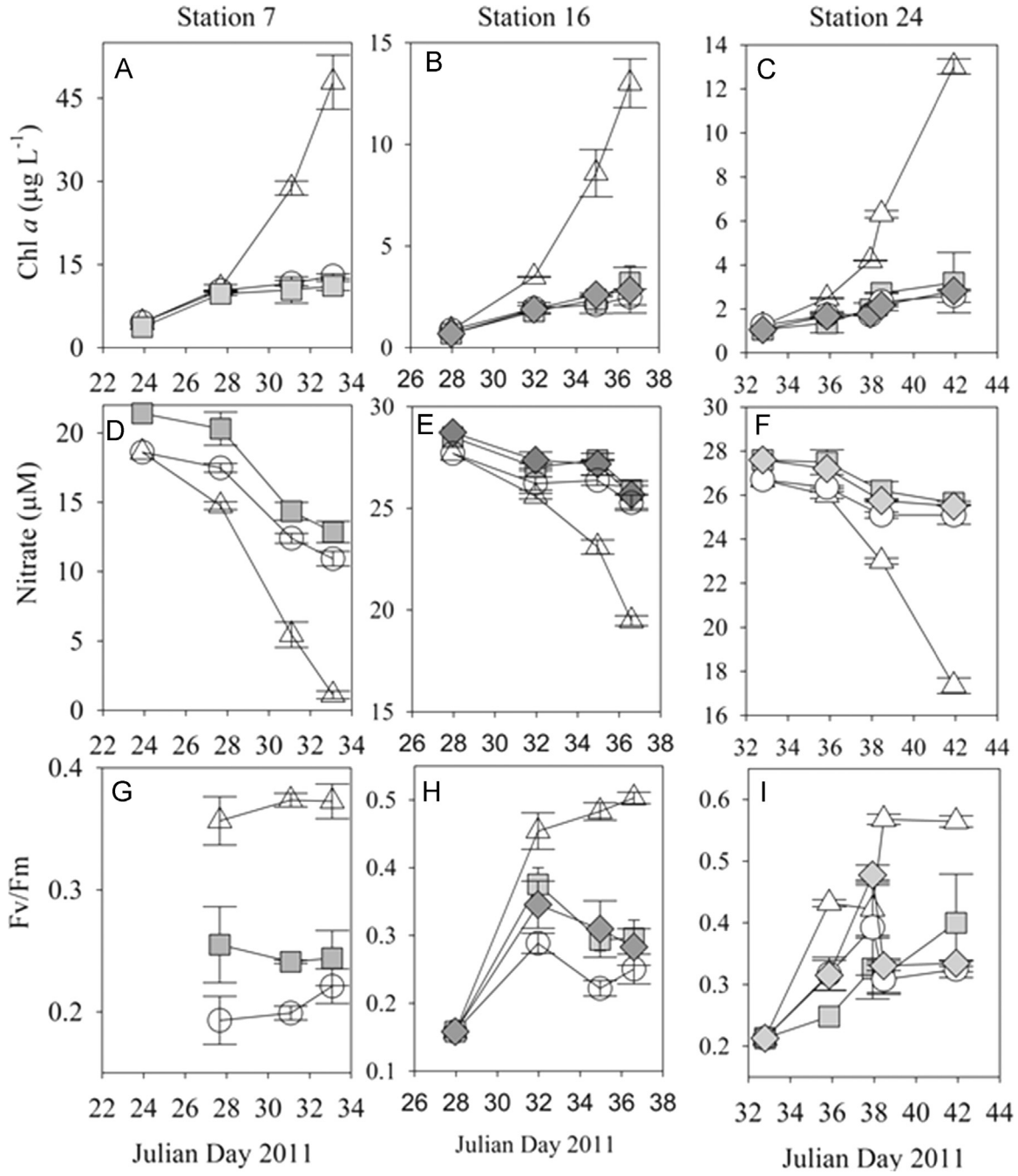

Fig. 7. Effect of various deep water additons and iron during incubation experiments. Rows 1–3 represent chl *a* accumulation, nitrate drawdown and variable fluorescence, respectively while columns 1–3 represent stations 7, 16 and 24. Open triangles and circles represent ferric chloride (1 nM addition) and control treatments, respectively. Grey squares represent 20% addition of filtered MCDW for stations 16 and 24 and deep water for station 7. For stations 16 and 24, grey diamonds indicate treatments amended with filtered CDW or unfiltered (raw) MCDW, respectively. Station 48 results are not shown here but all data are provided in Supplemental Table 3. Note that surface water and deep water amended treatments have differing starting chl *a* and nitrate concentrations, as expected.

4. Discussion

The dissolved Fe concentrations corresponding to the MCDW at WF stations 16, 24 and 41 were lower than that obtained at similar depths from offshore CDW sources (station 14; ~0.45 nM). Model results suggest that the MCDW waters found in the WF region are comprised of no more than ca. 35% CDW (Supplemental Fig. 3), suggesting that the MCDW waters at this location were diluted with Fe-poor waters, and implying that MCDW in the WF region is not serving as an exceptionally Fe-rich source. The presence of CDW tagged dye at CPB, along with the supporting physical data and model output, indicates the connection between the MCDW observed at WF and deep waters at Pennell Bank (Supplemental Fig. 3A and B). The lower dye concentration and higher iron concentration of the deep water at CPB relative to WF indicate that these waters were further modified by surrounding shelf water with elevated iron. The dynamics of the dye appearance and increasing concentrations over time is consistent with the counterclockwise flow along the 300 m isobath of Pennell Bank (Kohut et al., 2013), and also suggests a mechanism to inject deep waters onto more shallow regions of the bank.

The lower Fe content of these MCDW waters suggests at least three possibilities to explain the enhanced productivity observed on CPB. First, the vertical supply of Fe may be sufficient even at

Table 2
Incubation growth rate estimates based on chlorophyll *a* accumulation and nitrate drawdown. Expected Fe was calculated from dissolved Fe concentrations measured in surface and deep waters, and the contribution of 1 nM ferric chloride, where appropriate (Table 1, Figure 4). The range of values given for the MCDW treatment for station 16 reflects the variability in dissolved Fe concentration across the depth range at which Go-Flo bottles were fired. The value in parentheses for the unfiltered MCDW treatment also considers the particulate labile Fe, as measured in this MCDW (Lam et al., 2014). All growth rate measurements were from duplicate cubitainers, except the No Fe treatment for station 24 (n = 3). Abbreviations for incubation treatments include: Fe = 1 nM ferric chloride; 20% MCDW = 20% addition of Modified Circumpolar Deep Water (0.2 μm filtered, except as noted).

Treatment	Expected Fe (pM)				Chl *a*-specific growth (d^{-1})				Nitrate-specific growth (d^{-1})			
	Station 7	Station 16	Station 24	Station 48	Station 7	Station 16	Station 24	Station 48	Station 7	Station 16	Station 24	Station 48
No Fe	206	186	118	127	0.099 (0.016)	0.096 (0.020)	0.105 (0.026)	0.160 (0.0087)	0.085 (0.020)	0.117 (0.0092)	0.062 (0.012)	0.117 (0.0068)
Fe	1206	1186	1118	1127	0.258 (0.0054)	0.295 (0.015)	0.262 (0.0015)	0.365 (0.0092)	0.154 (0.0039)	0.210 (0.0056)	0.178 (0.0037)	0.275 (0.0017)
20% MCDW		193–200	130			0.150 (0.031)	0.128 (0.032)			0.125 (0.017)	0.0855 (0.0067)	
20% unfiltered MCDW			130 (330)				0.105 (0.004)				0.0885 (0.00060)	
20% deep water CDW	234	240			0.113 (0.017)	0.141 (0.038)			0.130 (0.0014)	0.107 (0.0028)		

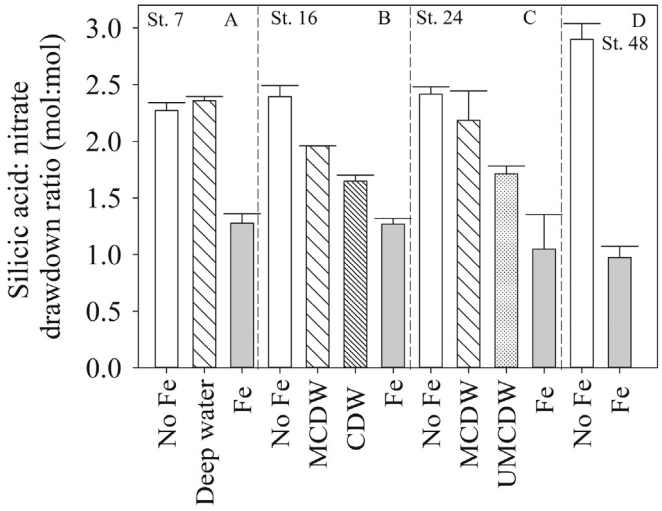

Fig. 8. Silicate:nitrate drawdown ratios in response to various deep water additions or ferric chloride. Panels A–D represent results from incubation stations 7, 16, 24 and 48 respectively. Symbols for "no Fe" treatments are hollow, while deep water treatments are hollow with wide cross hatches (MCDW or deep water collected on station), narrow cross hatches (CDW from station 14), or stippled (unfiltered, UMCDW). Ferric chloride treatments (Fe) are indicated in grey. Error bars represent standard deviations of values from replicate cubitainers. Of the planned comparisons tested, the drawdown ratios from ferric chloride treatments (all stations) and the unfiltered MCDW treatment (station 24) were significantly less ($p < 0.05$) than those of the no Fe controls.

modest dissolved concentrations observed below the bloom. The model calculations presented here suggest 2–15% of the demand at CPB stations may be supplied from vertical transport. Moreover, the dye concentrations in deep waters of CPB suggest ~20% of this deep water may be derived from offshore CDW. Second, particulate labile Fe pools (insofar as the acid lability approximates bioavailability) may partly fulfill the Fe demand (Boyd et al., 2010). We saw an effect of 0.2 nM particulate labile Fe addition on two of four metrics from station 24 incubations, but we cannot speculate on whether higher concentrations of particulate Fe would have elicited a more consistent response from all four metrics. Third, regeneration of Fe may occur on more rapid time scales than regeneration of nitrogen; to the extent that this occurs the calculated Fe demand may overestimate the actual demand for new Fe. Of course, factors other than Fe may be involved in explaining this enhanced productivity at CPB. Median mixed layer depths were similar among these stations (Table 1), suggesting differences in light regime may have only played a minor role.

Our model calculations implicitly include the contributions of any iron sources that may contribute to the dissolved inventory in the subsurface waters. This includes likely diagenetically supplied Fe (Marsay et al., 2014) from regions of the flow path on Pennell Bank where currents communicate with diagenetic sediments. This will be discussed in further detail in a companion paper that compares the physics, chemistry and biology and sediments of Mawson and Pennell Banks, motivated by the results presented here. These model results do not take into account the vertical supply of any particulate Fe that may be labile, while we recognize this could also be important (Boyd et al., 2010; Lam et al., 2014,).

Surface dissolved Fe concentrations within the study area were 0.12–0.21 pM, values which lead to modest to severe growth rate limitation in cultures of Southern Ocean diatoms (Timmermans et al., 2004). The phytoplankton in this region were dominated by diatoms (*Chaetoceros* and *Pseudo-nitzchia,* and to lesser extents *Corethron* and *Fragilariopsis*; as assessed by 18S ribosomal DNA sequencing; Kustka et al. (2015)). These low concentrations in diatom dominated assemblages suggest Fe was limiting growth and

Table 3
Biomass specific and depth integrated productivity and subsequent required Fe supply and upwelling velocity. Net productivity was determined over 24 h, as indicated in more detail in Section 2. Required vertical supply rates to sustain blooms at various locations, in the absence of regeneration within the mixed layer, assuming an Fe:C demand calculated from integrated surface water Fe and nitrate depletion or a fixed ratio of 7 μmol:mol. CPB and NPB refer to Central Pennell Bank and Northern Pennell Bank, respectively while WF refers to the western flank of Pennell Bank. Location averaged Fe:C demands refer to the averages for CPB and NPB stations.

Station	Alpha (g C g chl a^{-1} h^{-1}) (μmol m^{-2} s^{-1})$^{-1}$	P^b_{max} (g C g chl a^{-1} h^{-1})	Net production (mmol C m^{-2} d^{-1})	Apparent Fe:C demand (μmol mol^{-1})	Location average Fe:C (μmol mol^{-1})	Areal Fe demand (nmol Fe m^{-2} d^{-1})	Subsurface dFe (nM)	Vertical demand (m d^{-1})
7	0.102 (0.028)	4.21 (0.40)	457	2.00	1.74	794–3199	0.286	2.8–11.2
16	0.037 (0.009)	1.79 (0.14)	87	0.76	1.51	131–609	0.198	0.7–3.1
24	0.044 (0.015)	1.53 (0.19)	105	2.48	1.51	158–735	0.185	0.9–4.0
41	0.032 (0.008)	1.63 (0.14)	56	1.28	1.51	84–392	0.122	0.7–3.2
48	0.036 (0.007)	1.78 (0.12)	91	2.06	2.06	187–637	0.219	0.9–2.9
61/64	0.113 (0.027)	3.20 (0.29)	300	1.48	1.74	521–2100	0.217	2.4–9.7

Table 4
Estimated regional upwelling rates based on increased surface water dye concentrations over time. CPB, NPB and WF indicate Central Pennell Bank, Northern Pennell Bank, and Western Flanking regions (as identified in Fig. 1B). Dye concentrations in surface and sub-surface strata (0–100 m and 100–200 m, respectively) were sampled daily from neutrally buoyant drifters, as described in greater detail in text.

Region	65 day integrated rate (d^{-1})	Median daily rate (d^{-1})	65 day integrated velocity (m d^{-1})	Median daily velocity (m d^{-1})
CPB	4.29×10^{-3}	1.80×10^{-3}	0.43	0.18
NPB	-4.50×10^{-3}	-1.03×10^{-2}	−0.45	−1.0
WF	-3.66×10^{-3}	-3.04×10^{-3}	−0.36	−0.30

primary productivity, consistent with earlier observations in the region (Sedwick and DiTullio, 1997; Sedwick et al., 2000; Olson et al., 2000). The low F_v/F_m values (0.24–0.37) across the region are also indicative of widespread *in situ* Fe limitation. However, interpreting in situ F_v/F_m can be equivocal and requires some further discussion. Strzepek et al. (2012) showed that Fe-replete cultures of Southern Ocean diatoms may have F_v/F_mvalues as low as 0.25–0.3 in a manner dependent on light acclimation history. While we only considered underway F_v/F_m values observed under low light conditions, this does not strictly consider the integrated light history of the populations.

Our incubations show that F_v/F_m values, Si:N removal ratios, and growth rate responses are all consistent with growth rate limitation by Fe across the study area. The changes in F_v/F_m during incubations also support the interpretation of *in situ* iron limitation. While *in situ* values were similar to those of Fe replete cultures of Southern Ocean diatoms (Strzepek et al., 2012), the increased differences between F_v/F_m values of Fe amended and control treatments during the course of the incubations (Table 3, Fig. 7) are consistent with in situ Fe limitation. The incubation irradiance (40 μmol photon m^{-2} s^{-1}) was similar to that required

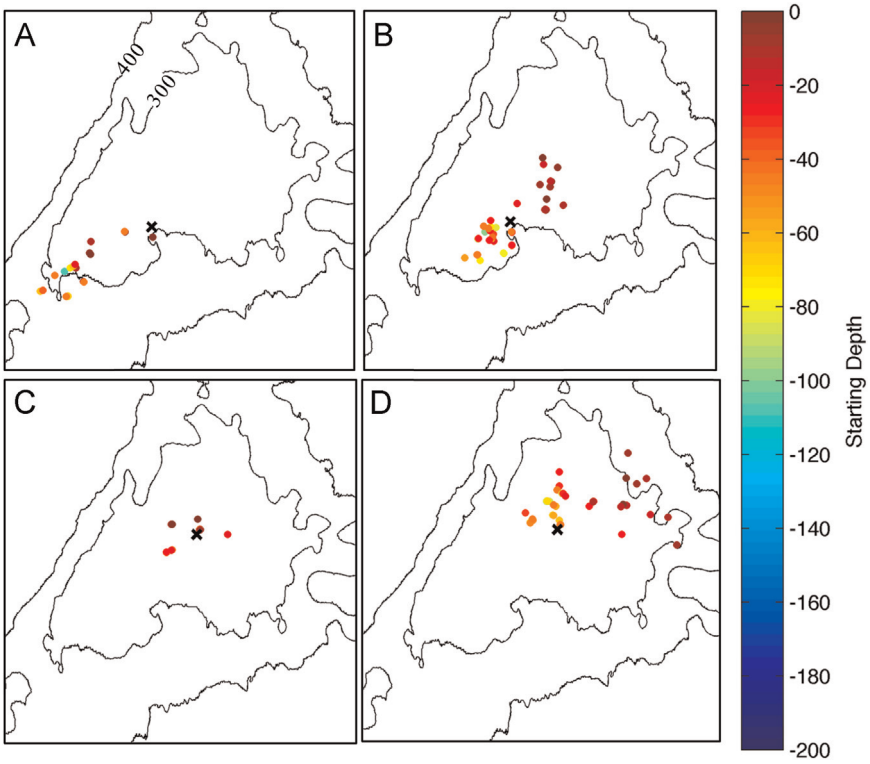

Fig. 9. Hindcast trajectories of neutral density drifters found in the top 100 m of the water column within the vicinity of stations 7 and 48 in late summer 2011. Color coded symbols represent the starting locations and depths of drifters located in the upper 100 m and within 10 km of station (cross hatched symbol), 14 days prior to the specified date. In each panel, station locations are indicated with a cross-hatched symbol, and the 300 and 400 m isobaths of Pennell Bank are labeled in panel A. (A) Starting location of drifters located in surface waters near station 7 on 31 Jan 2011. (B) As in panel A, but on 14 Feb 2011. (C) As in panel A, except near station 48. (D) As in panel A, except near station 48 on 14 Feb 2011.

for saturation of photosynthesis (42 ± 9 μmol photon m^{-2} s^{-1}; from α and P_b^{max} in Table 3).

The F_v/F_m response after 9 days of high Fe treatment at station 7 was lower than values observed for the same treatment in the other three incubations (0.373 vs. 0.536 ± 0.031). This is not likely due to differences in Fe status among Fe amended populations, considering that growth rates and Si:N removal ratios were similar (Table 2, Fig. 8). Rather, the lower than expected variable to maximum fluorescence value may simply reflect differences in phytoplankton assemblages and potential differences in the recovery kinetics of F_v/F_m after Fe addition. Station 7 was dominated (57% of phytoplankton 18S copy numbers) by *Chaetoceros sp.* clades, with minimal (2%) contributions from *Pseudonitzschia* (Kustka et al., 2015). In contrast, stations 24 and 48 had lesser relative abundances of *Chaetoceros* (18% and 37%) and increases in *Pseudonitzschia* (8% and 28%). Therefore, these results might be explained by slower kinetics for recovery of F_v/F_m in *Chaetoceros sp.* compared to other species.

The circulation model has been shown to accurately simulate the observed pathways of CDW intrusions onto and across the continental shelf (Dinniman et al., 2011) and a comparison of the model MCDW volume transport in the WF region (0.22 ± 0.03 Sv) over a two week period (27 Jan–9 Feb 2011) with that estimated from a mooring (0.24 Sv; Kohut et al. (2013)) implies that, at least around the time of these observations, the modeled MCDW transport along the WF region is reasonable. However, it has also been shown that near Pennell Bank the modeled mixed layer depth in summer is often too shallow and the maximum temperatures of the MCDW intrusions in the WF region are too warm (McGillicuddy et al., in press both of which imply that there may be too little mixing of MCDW (at least in the WF region) in the model as it intrudes onto the shelf. Over the bank, the modeled hydrography accurately reproduced the depth of the observed mixed layer, however the modeled stratification in the upper 50 m of the model was stronger than the observed stratification due to a fresher surface layer in the model. We therefore use the model simulations to provide an estimate of the scale of the vertical supply to provide context on the potential relative rates across this region.

There were ~five-fold ranges in chl *a* and net primary production (Table 3) across the Pennell Bank region, where iron limitation was widespread. These observations are consistent with spatially variable vertical Fe supply rates that are matched by the demand for phytoplankton growth, although the effect of iron-light interactions (Alderkamp et al., 2012) or grazing (Landry et al., 1997) cannot be discounted. The upwelling of Fe in the CPB region is adequate to supply at least some of the Fe required for the observed high productivity. The model results suggest that upwelling of subsurface waters is more pronounced at CPB than other regions. The relative differences in calculated regional Fe supply rates are consistent with differences in demand and suggest that shallow mixed layers in the WF and NPB regions do not result in the same enhanced productivity as observed at CPB stations because the rate of upwelling in the former regions may not supply adequate iron.

While the highly productive area in the CPB region is consistent with the predicted vertical supply of Fe, the paramount role of Fe recycling must be recognized. Indeed, the proportion of productivity that depends on new Fe may be as low as ~6% in the most Fe limited regions (Boyd et al., 2005). This capacity for recycling may explain the significantly higher calculated Fe demands relative to the predicted supplies; perhaps even more dramatic at WF and NPB stations where modeled vertical velocities were not positive (likely reflecting some of the limitations of the model described above). Of course, this difference may also arise from the inherent assumptions in both our supply and demand calculations. Nonetheless, even with effective Fe recycling, an increases supply of new Fe should still lead to increases in productivity in these persistently Fe limited regions.

While phytoplankton biomass levels in the northern Ross Sea are lower than those observed in the southern portion, the enhanced standing stocks observed on Pennell Bank suggest that the broad patterns seen over the entire continental shelf may reflect spatial variability of meso- and sub-mesoscale factors that alleviate growth limitation. Circulation patterns around topographically dynamic features such as banks can alter input of Fe through both increased upwelling rates and higher concentrations of iron. The modeled rates of Fe inputs are consistent with the estimated iron demands. While other areas of the Ross Sea also have significant spatial variability induced by different mechanisms (e.g., irradiance limitation induced by deep vertical mixing; Smith and Jones, 2014)], a more clear understanding of the physical factors controlling phytoplankton growth will advance our understanding of the mechanisms responsible for generating the spatial variations in phytoplankton biomass throughout the ocean.

Acknowledgments

This work was supported through the following awards from the NSF Division of Polar Programs: 0839039 (A.B.K. and J.T.K.), 0838921 (P.J.L.), 0839024 (C.I.M.), 0839062 (J. Sarmiento), and 0838980 (W.O.S.). We are grateful to Mariko Hatta, Ashley New and Katie Watkins-Brandt for assistance during the cruise, and to Laura Palamara for assistance with post-cruise data processing .

Appendix A. Supplementary material

Supplementary data associated with this article can be found in the online version at http://dx.doi.org/10.1016/j.dsr.2015.08.012.

References

Alderkamp, A.C., Kulk, G., Buma, A.G.J., Visser, R.J.W., Van Dijken, G.L., Mills, M.M., Arrigo, K.R., 2012. The effect of iron limitation on the photophysiology of *Phaeocystis Antarctica* (Prymnesiophyceae) and *Fragilariopsis cylindricus* (Bacillariophyceae) under dynamic irradiance. J. Phycol. 48, 45–59.

Armstrong, F.A.J., Stearns, C.R., Strickland, J.D.H., 1967. The measurement of upwelling and subsequent biological processes by means of the Technicon AutoAnalyzer and associated equipment. Deep Sea Res. Oceanogr. Abstr. 14 (3), 381–389.

Arrigo, K.R., Van Dijken, G.L., 2004. Annual changes in sea-ice, chlorophyll *a*, and primary production in the Ross Sea, Antarctica. Deep. Res. Part II Top. Stud. Oceanogr. 51, 117–138.

Arrigo, K.R., van Dijken, G.L., Bushinsky, S., 2008. Primary production in the Southern Ocean, 1997–2006. J. Geophys. Res. Ocean 113, 1997–2006.

Arrigo, K.R., Worthen, D., Schnell, A., Lizotte, M.P., 1998. Primary production in Southern Ocean waters. J. Geophys. Res. C 103, 15587–15600.

Arrigo, K.R., Robinson, D.H., Worthen, D.L., Dunbar, R.B., DiTullio, G.R., VanWoert, M., Lizotte, M.P., 1999. Phytoplankton community structure and the drawdown of nutrients and CO_2 in the Southern Ocean. Science 283, 365–367.

Atlas, E.L., Hager, S.W., Gordon, L.I., Park, P.K., 1971. A Practical Manual for the Use of the Technicon Autoanalyzer in Seawater Nutrient Analyses; Revised. Oregon State University, Corvallis, Technical Report 215.

Boyd, P.W., Ibisanmi, E., Sander, S.G., Hunter, K.A., Jackson, G.A., 2010. Remineralization of upper ocean particles: implications for iron biogeochemistry. Limnol. Oceanogr. 55, 1271–1288.

Boyd, P.W., Law, C.S., Hutchins, D.A., Abraham, E.R., Croot, P.L., Ellwood, M., Frew, R. D., Hadfield, M., Hall, J., Handy, S., Hare, C., Higgins, J., Hill, P., Hunter, K.A., LeBlanc, K., Maldonado, M.T., McKay, R.M., Mioni, C., Oliver, M., Pickmere, S., Pinkerton, M., Safi, K., Sander, S., Sanudo-Wilhelmy, S.A., Smith, M., Strzepek, R., Tovar-Sanchez, A., Wilhelm, S.W., 2005. Fe Cycle: attempting an iron biogeochemical budget from a mesoscale SF_6 tracer experiment in unperturbed low iron waters. Glob. Biogeochem. Cycles 19, 1–13.

De Boyer Montégut, C., Madec, G., Fischer, A.S., Lazar, A., Iudicone, D., 2004. Mixed layer depth over the global ocean: an examination of profile data and a profile-based climatology. J. Geophys. Res. C Ocean 109, 1–20.

Budgell, W.P., 2005. Numerical simulation of ice–ocean variability in the Barents Sea region. Ocean Dyn. 55, 370–387.
Castro-Morales, K., Kaiser, J., 2012. Using dissolved oxygen concentrations to determine mixed layer depths in the Bellingshausen Sea. Ocean Sci. 8, 1–10.
Cetinić, I., Perry, M.J., Briggs, N.T., Kallin, E., D'Asaro, E.A., Lee, C.M., 2012. Particulate organic carbon and inherent optical properties during 2008 North Atlantic bloom experiment. J. Geophys. Res. Ocean 117. http://dx.doi.org/10.1029/2011JC007771.
Cochlan, W.P., Bronk, D.A., Coale, K.H., 2002. Trace metals and nitrogenous nutrition of Antarctic phytoplankton: experimental observations in the Ross Sea. Deep. Res. Part II Top. Stud. Oceanogr. 49, 3365–3390.
Dee, D.P., Uppala, S.M., Simmons, A.J., Berrisford, P., Poli, P., Kobayashi, S., Andrae, U., Balmaseda, M.A., Balsamo, G., Bauer, P., Bechtold, P., Beljaars, A.C.M., van de Berg, L., Bidlot, J., Bormann, N., Delsol, C., Dragani, R., Fuentes, M., Geer, A.J., Haimberger, L., Healy, S.B., Hersbach, H., Hólm, E.V., Isaksen, L., Kållberg, P., Köhler, M., Matricardi, M., Mcnally, A.P., Monge-Sanz, B.M., Morcrette, J.J., Park, B.K., Peubey, C., de Rosnay, P., Tavolato, C., Thépaut, J.N., Vitart, F., 2011. The ERA-Interim reanalysis: configuration and performance of the data assimilation system. Q. J. R. Meteorol. Soc. 137, 553–597.
Dinniman, M.S., Klinck, J.M., Smith, W.O., 2003. Cross-shelf exchange in a model of the Ross Sea circulation and biogeochemistry. Deep-Sea Res. II 50, 3103–3120.
Dinniman, M.S., Klinck, J.M., Smith, W.O., 2007. Influence of sea ice cover and icebergs on circulation and water mass formation in a numerical circulation model of the Ross Sea, Antarctica. J. Geophys. Res. Ocean 112, 1–13.
Dinniman, M.S., Klinck, J.M., Smith, W.O., 2011. A model study of Circumpolar Deep Water on the West Antarctic Peninsula and Ross Sea continental shelves. Deep Sea Res. Part II Top. Stud. Oceanogr. 58, 1508–1523.
Gardner, W.D., Mishonov, A.V., Richardson, M.J., 2006. Global POC concentrations from in-situ and satellite data. Deep Sea Res. Part II Top. Stud. Oceanogr. 53, 718–740.
Gorbunov, M., Falkowski, P., 2004. Fluorescence induction and relaxation (FIRe) technique and instrumentation for monitoring photosynthetic processes and primary production in aquatic. In: Proceedings of the 13th International Congress of Photosynthesis, pp. 29–31.
Haidvogel, D.B., Arango, H., Budgell, W.P., Cornuelle, B.D., Curchitser, E., Di Lorenzo, E., Fennel, K., Geyer, W.R., Hermann, A.J., Lanerolle, L., Levin, J., McWilliams, J.C., Miller, A.J., Moore, A.M., Powell, T.M., Shchepetkin, A.F., Sherwood, C.R., Signell, R.P., Warner, J.C., Wilkin, J., 2008. Ocean forecasting in terrain-following coordinates: formulation and skill assessment of the Regional Ocean Modeling System. J. Comput. Phys. 227, 3595–3624.
Halsey, K.H., Milligan, A.J., Behrenfeld, M.J., 2011. Linking time-dependent carbon-fixation efficiencies in *Dunaliella tertiolecta* (Chlorophyceae) to underlying metabolic pathways. J. Phycol. 47, 66–76.
Hatta, M., Measures, C.I., Selph, K.E., Zhou, M., Hiscock, W.T., 2013. Iron fluxes from the shelf regions near the South Shetland Islands in the Drake Passage during the austral-winter 2006. Deep Sea Res. II 90, 89–101.
Hatta, M., Measures, C.I., Wu, J.F., Roshan, S., Fitzsimmons, J.N., Sedwick, P., Morton, P., 2015. An overview of dissolved Fe and Mn distributions during the 2010–2011 US GEOTRACES north Atlantic cruises: GEOTRACES GA03. Deep Sea Res. II 116, 117–129.
Hiscock, M.R., Marra, J., Smith, W.O., Goericke, R., Measures, C., Vink, S., Olson, R.J., Sosik, H.M., Barber, R.T., 2003. Primary productivity and its regulation in the Pacific Sector of the Southern Ocean. Deep-Sea Res. II 50, 533–558.
Holland, D.M., Jenkins, A., 1999. Modeling thermodynamic ice–ocean interactions at the base of an ice shelf. J. Phys. Oceanogr. 29, 1787–1800.
Hunter, J.R., Craig, P.D., Phillips, H.E., 1993. On the use of random walk models with spatially variable diffusivity. J. Comput. Phys. 106, 366–376.
Jacobs, S.S., Giulivi, C.F., 1998. Interannual ocean and sea ice variability in the Ross Sea. In: Jacobs, S.S., Weiss, R.F. (Eds.), Ocean, Ice and Atmosphere Interactions at the Continental Margin, Antarctic Research Series 75. American Geophysical Union, Washington, DC, pp. 135–150.
Kohut, J., Hunter, E., Huber, B., 2013. Small-scale variability of the cross-shelf flow over the outer shelf of the Ross Sea. J. Geophys. Res. Ocean 118, 1863–1876.
Kustka, A.B., Jones, B.M., Field, M.P., Hatta, M., Milligan, A.J., 2015. The influence of iron and siderophores on marine phytoplankton growth rates and community composition in the Ross Sea. Mar. Chem. **173**:195-207.
Landry, M.R., Barber, R.T., Bidigare, R.R., Chai, F., Coale, K.H., Dam, H.G., Lewis, M.R., Lindley, S.T., McCarthy, J.J., Roman, M.R., Stoecker, D.K., Verity, P.G., White, J.R., 1997. Iron and grazing constraints on primary production in the central equatorial Pacific: an EqPac synthesis. Limnol. Oceanogr. 42, 405–418.
Lam, P.J., Ohnemus, D.C., Swartz, J., Aurol, M.E., Kohut, J., Hatta, M., 2014. Sediments as a source of iron in the Ross Sea: sediment characteristics and particulate iron. In: Annual Ocean Sciences Meeting, Honolulu, HI.
Lee, K., Tong, L.T., Millero, F.J., Sabine, C.L., Dickson, A.G., Goyet, C., Park, G.-H., Wanninkhof, R., Feely, R.A., Key, R.M., 2006. Global relationships of total alkalinity with salinity and temperature in surface waters of the world's oceans. Geophys. Res. Lett. 33, L19605.
Lorbacher, K., Dommenget, D., Niiler, P.P., Köhl, A., 2006. Ocean mixed layer depth: a subsurface proxy of ocean–atmosphere variability. J. Geophys. Res. Ocean 111, 1–22.
Marsay, C.M., Sedwick, P.N., Dinniman, M.S., Barrett, P.M., Mack, S.L., McGillicuddy, D.J., 2014. Estimating the benthic efflux of dissolved iron on the Ross Sea continental shelf. Geophys. Res. Lett. 41, 7576–7583.
Martin, J.H., Gordon, R.M., Fitzwater, S.E., 1991. The case for iron. Limnol. Oceanogr. 36, 1793–1802.
McGillicuddy, D.J., Sedwick, P.N., Dinniman, M.S., Arrigo, K.R., Bibby, T.S., Greenan, B. J.W., Hofmann, E.E., Klinck, J.M., Smith, W.O., Mack, S.L., Marsay, C.M., Sohst, B. M., van Dijken, G.L. Iron supply and demand in an Antarctic shelf ecosystem. Geophys. Res. Lett., in press.
Measures, C.I., Yuan, J., Resing, J.A., 1995. Determination of iron in seawater by flow injection analysis using in-line preconcentration and spectrophotometric detection. Mar. Chem. 50, 3–12.
Measures, C.I., Landing, W.M., Brown, M.T., Buck, C.S., 2008. A commercially available rosette system for trace metal clean sampling. Limnol. Oceanogr. Methods 6, 384–394.
Milne, A., Landing, W., Bizimis, M., Morton, P., 2010. Determination of Mn, Fe, Co, Ni, Cu, Zn, Cd and Pb in seawater using high resolution magnetic sector inductively coupled mass spectrometry (HR-ICP-MS). Anal. Chim. Acta 665, 200–207.
Olson, R.J., Sosik, H.M., Chekalyuk, A.M., Shalapyonok, A., 2000. Effects of iron enrichment on phytoplankton in the Southern Ocean during late summer: active fluorescence and flow cytometric analyses. Deep-Sea Res. II 47, 3181–3200.
Orsi, A.H., Wiederwohl, C.L., 2009. A recount of Ross Sea waters. Deep. Res. Part II Top. Stud. Oceanogr. 56, 778–795.
Padman, L., Fricker, R., Coleman, S., Howard, Erofeeva, S., 2002. A new tidal model for the Antarctic ice shelves and seas. Ann. Glaciol. 34, 247–254.
Park, Y.H., Gamberoni, L., Charriaud, E., 1993. Frontal structure, water masses, and circulation in the Crozet Basin. J. Geophys. Res. 98 (C7), 12361–12385.
Porra, R.J., Thompson, W.A., Kriedemann, P.E., 1989. Determination of accurate extinction coefficients and simultaneous equations for assaying chlorophylls *a* and *b* extracted with four different solvents: verification of the concentration of chlorophyll standards by atomic absorption spectroscopy. Biochim. Biophys. Acta 975, 384–394.
Prézelin, B.B., Hofmann, E.E., Mengelt, C., Klinck, J.M., 2000. The linkage between Upper Circumpolar Deep Water (UCDW) and phytoplankton assemblages on the west Antarctic Peninsula continental shelf. J. Mar. Res. 58, 165–202.
Sedwick, P.N., DiTullio, G.R., 1997. Regulation of algal blooms in Antarctic Shelf Waters by the release of iron from melting sea ice. Geophys. Res. Lett. 24, 2515.
Sedwick, P.N., DiTullio, G.R., Mackey, D.J., 2000. Iron and manganese in the Ross Sea, Antarctica: seasonal iron limitation in Antarctic shelf waters. J. Geophys. Res. Oceans 105, 11321–11336.
Sedwick, P.N., Marsay, C.M., Sohst, B.M., Aguilar-Islas, A.M., Lohan, M.C., Long, M.C., Arrigo, K.R., Dunbar, R.B., Saito, M.A., Smith, W.O., DiTullio, G.R., 2011. Early season depletion of dissolved iron in the Ross Sea polynya: implications for iron dynamics on the Antarctic continental shelf. J. Geophys. Res. Ocean 116, 1–19.
Shchepetkin, A.F., McWilliams, J.C., 2009. Correction and commentary for "Ocean forecasting in terrain-following coordinates: formulation and skill assessment of the regional ocean modeling system by Haidvogel et al. J. Comp. Phys. 227, 3595–3624, J. Comput. Phys. 228: 8985–9000.
Slade, W.H., Boss, E., Dall'olmo, G., Langner, M.R., Loftin, J., Behrenfeld, M.J., Roesler, C., Westberry, T.K., 2010. Underway and moored methods for improving accuracy in measurement of spectral particulate absorption and attenuation. J. Atmos. Ocean. Technol. 27, 1733–1746.
Smith, W.O., Asper, V.L., 2001. The influence of phytoplankton assemblage composition on biogeochemical characteristics and cycles in the southern Ross Sea, Antarctica. Deep-Sea Res. I 48, 137–161.
Smith, W.O., Comiso, J.C., 2008. Influence of sea ice on primary production in the Southern Ocean: a satellite perspective. J. Geophys. Res. 113, 1–19.
Smith, W.O., Marra, J., Hiscock, M.R., Barber, R.T., 2000. The seasonal cycle of phytoplankton biomass and primary productivity in the Ross Sea, Antarctica. Deep Sea Res. Part II Top. Stud. Oceanogr. 47, 3119–3140.
Smith, W.O., Shields, A.R., Dreyer, J.C., Peloquin, J.A., Asper, V., 2011. Interannual variability in vertical export in the Ross Sea: magnitude, composition, and environmental correlates. Deep. Res. Part I Oceanogr. Res. Pap. 58, 147–159.
Smith, W.O., Goetz, K.T., Kaufman, D.E., Queste, B.Y., Asper, V., Costa, D.P., Dinniman, M.S., Friedrichs, M.A.M., Hofmann, E.E., Heywood, K.J., Klinck, J.M., Kohut, J.T., Lee, C.M., 2014. Multiplatform, Multidisciplinary Investigations of the Impacts of Modified Circumpolar Deep Water in the Ross Sea, Antarctica. Oceanography 27, 180–185.
Smith, W.O., Jones, R.M., 2014. Vertical mixing, critical depths, and phytoplankton growth in the Ross Sea. ICES J. Mar. Sci. http://dx.doi.org/10.1093/icesjms/fsu234.
Strzepek, R.F., Hunter, K.A., Frew, R.D., Harrison, P.J., Boyd, P.W., 2012. Iron-light interactions differ in Southern Ocean phytoplankton. Limnol. Oceanogr. 57, 1182–1200.
Suggett, D.J., Moore, C.M., Hickman, A.E., Geider, R.J., 2009. Interpretation of fast repetition rate (FRR) fluorescence: signatures of phytoplankton community structure versus physiological state. Mar. Ecol. Prog. Ser. 376, 1–19.
Timmermans, K.R., van der Wagt, B., de Baar, H.J.W., 2004. Growth rates, half-saturation constants, and silicate, nitrate, and phosphate depletion in relation to iron availability of four large, open-ocean diatoms from the Southern Ocean. Limnol. Oceanogr. 49, 2141–2151.
Vink, S., Boyle, E.A., Measures, C.I., Yuan, J., 2000. Automated high resolution determination of the trace elements iron and aluminum in the surface ocean using a towed fish coupled to flow injection analysis. Deep Sea Res. I 47, 1141–1156.
Visser, A.W., 1997. Using random walk models to simulate the vertical distribution of particles in a turbulent water column. Mar. Ecol. Prog. Ser. 158, 275–281.
Walsby, A.E., 1997. Numerical integration of phytoplankton photosynthesis through time and depth in a water column. New Phytol. 136, 189–209.
White, A.E., Milligan, A.J., Kustka, A.B., 2014. Primary productivity in the Ross Sea: results from 14C tracer measurements and models based on continuous flow through data. Annual Ocean Sciences Meeting, Honolulu, HI.

White, A.E., Milligan, A.J., Kustka, A.B. 2014. Primary productivity in the Ross Sea: results from ^{14}C tracer measurements and models based on continuous flow through data. Annual Ocean Sciences Meeting, Honolulu, HI. White, A.E., Kustka, A.B., Watkins-Brandt, K., Milligan, A.J., 2015. Primary production in the Ross Sea using 14C and optical methods. Deep Sea Res. (in preparation)
Whitworth III, T., Nowlin Jr., W.D., 1987. Water masses and currents of the Southern Ocean at the Greenwich Meridian. J. Geophys. Res. 92 (C6), 6462–6476.
Winton, V.H.L., Dunbar, G.B., Bertler, N.A.N., Millet, M.A., Delmonte, B., Atkins, C.B., Chewings, J.M., Andersson, P., 2014. The contribution of aeolian sand and dust to iron fertilization of phytoplankton blooms in southwestern Ross Sea, Antarctica. Global Biogeochem. Cycles 28, 423–436.